Inorganic Chemistry

pubs.acs.org/IC

Article

Spectroscopic Identification of the Dinitrogen Fixation and Activation by Metal Carbide Cluster Anions PtC_n^- (n = 4–6)

Shihu Du, Xuegang Liu, Bangmin Ju, Jumei Zhang, Jinghan Zou, Gang Li, Hongjun Fan, Hua Xie,* and Ling Jiang

Cite This: *Inorg. Chem.* 2023, 62, 170–177

Read Online

ACCESS | Metrics & More | Article Recommendations | Supporting Information

ABSTRACT: Nitrogen fixation is confronted with great challenges in the field of chemistry. Herein, we report that single metal carbides PtC_n^- and $PtC_nN_2^-$ (n = 4–6) are indispensable intermediates in the process of nitrogen fixation by mass spectrometry coupled with anionic photoelectron spectroscopy, quantum chemical calculations, and simulated density-of-state spectra. The most stable isomers of these cluster anions are characterized to have linear chain structures. The fixation and activation of dinitrogen are facilitated by the charge transfer from Pt and C_n to N_2. The significance of π back-donation of the 5d orbital of the Pt atom to the antibonding π orbits of N_2 for dinitrogen fixation and activation is discussed in detail. This study not only provides a theoretical basis at the molecular level for the activation of dinitrogen by mononuclear metal carbide clusters but also provides a new paradigm for dinitrogen fixation.

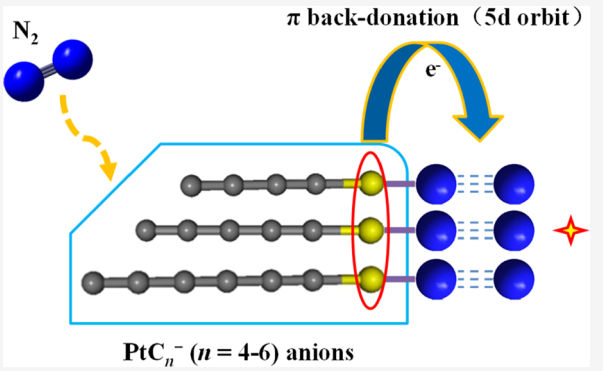

1. INTRODUCTION

The fixation and activation of nitrogen holds widespread applications in contemporary society, but it has confronted with rigorous challenges.[1,2] As an abundant and easily accessible resource, nitrogen becomes one of the raw materials for the synthetic ammonia industry. However, it is still a predicament to achieve the aim of breaking the N≡N triple bond under mild conditions.[3−6] It is well known that metal nitrides play a vital function in the development of high hardness materials and high refractories.[7] Several small transition metal nitrides, such as Zr_3N_4, Hf_3N_4, and so on,[8] have been synthesized under high pressure. Meanwhile, the synthesis of chemical raw materials into pharmaceutical products and chemical products (urea, etc.) is inseparable from the effect of metal carbonitride, such as the application of C−N bond coupling[9−15] and so forth. For the application of materials and technology, it is an inevitable trend to develop new nitride composites with fine structure property relationships.

In the condensed phase system, the experimental conditions are easily affected by the external environment, and so, the reaction mechanism cannot be clearly understood. In this context, the cluster model, as a method that is readily generated and has appropriate characteristics to study chemical reactions and reveal related mechanisms, emerges as the times require.[16−19] Previous studies demonstrated that most of the products obtained from the reaction of nitrogen with metal compounds exist in the modality of physical adsorption or chemical adsorption,[20−30] and only minority can fully activate nitrogen.[31,32]

Theoretical studies of the nitrogen activation mechanism revealed that the d-orbital electrons of the metal atom (adsorption site) back-donate to the antibonding π orbital of N_2,[33−35] with which transition metal atoms with 3d orbitals are widely used to immobilize and activate nitrogen in many applications.[36−38] Similarly, π back-donation was also observed from the occupied 4d orbitals of transition metal atoms into the π^* orbits of N_2.[39] Nevertheless, there are few reports on the dinitrogen activation by the 5d metals.[40−43] In addition, the special phenomenon that σ donation acts as the main function to activate dinitrogen has also been discovered.[44] The platinum carbides were proposed to be able to activate dinitrogen. In order to understand the activation mechanism of dinitrogen by the 5d metals, the platinum carbide clusters were selected as a model system to study the immobilization and activation of dinitrogen.

Received: September 5, 2022
Published: December 27, 2022

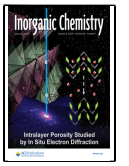

2. EXPERIMENTAL AND COMPUTATIONAL METHODS

The experiments were carried out using a homemade instrument, which included a laser vaporization source and a dual-channel time-of-flight mass spectrometer. Details of the apparatus have been described elsewhere,[45] and only a brief description is given below. The PtC_n^- (n = 4−6) anions were produced by laser vaporization of platinum−carbon mixture target (mole ratio, M/C = 1:5) with a pure helium carrier gas. $PtC_nN_2^-$ (n = 4−6) anions were produced by laser vaporization of platinum−carbon mixture target (mole ratio, M/C = 1:5) in the presence of helium carrier gas seeded with 5% N_2. The typical stagnation pressure of the carrier gas was about 2−5 atm. After cooling and expansion into the source chamber, the anions of interest were mass-selected by a Wiley−McLaren time-of-flight mass spectrometer and then introduced into the photodetachment region and interacted with laser beams of 266 nm (4.661 eV). The photoelectrons were mapped onto a detector consisting of a microchannel plate and a phosphor screen. The two-dimensional images on the phosphor screen were recorded by a charge-coupled device camera. Each image was obtained by accumulating 10,000−50,000 laser shots at a 10 Hz repetition rate. All of the raw images were reconstructed using the basis set expansion inverse Abel transform method (BASEX). The photoelectron spectra were calibrated using the known spectrum of Au^-. The energy resolution was better than 5%, corresponding to 50 meV at electron kinetic energy of 1 eV.

In order to elucidate the electronic and geometrical structures of PtC_n^- and $PtC_nN_2^-$ (n = 4−6), theoretical calculations were performed using the Gaussian 09 program.[46] The structures were optimized with density functional theory using the B3LYP function together with the basis set of aug-cc-pVTZ for C and N and aug-cc-pVTZ-PP for Pt atom.[47−49] Harmonic frequency analysis was carried out to make sure that the obtained structures were real minima on the potential energy surfaces. Theoretically, the vertical detachment energy (VDE) was calculated as the difference in energy between the neutral and anionic species based on the optimized anionic geometry, and the adiabatic detachment energy (ADE) was calculated as the difference in energy between the neutral and anion both at their optimized geometries. The zero-point-energy corrections were considered in the total energy of each cluster isomer for relative energy and ADE calculations. To understand the structure of $PtC_nN_2^-$ (n = 4−6) clusters, the canonical molecular orbital (CMO) analysis, Wiberg bond orders of N−N bond, and natural population analysis (NPA) of $PtC_nN_2^-$ (n = 4−6) were performed with NBO version 3.1 program[50] implemented in the Gaussian 09 package.

3. RESULTS AND ANALYSIS

3.1. Photoelectron Spectroscopy. The mass spectra of PtC_n^- and $PtC_nN_2^-$ (n = 4−6) clusters are shown in Figure S1. The upper part of Figure S1 shows the products PtC_n^- (n = 0−14) obtained with pure helium as the carrier gas. The product $PtC_nN_2^-$ (n = 4−6) was obtained with helium containing 5% nitrogen as the carrier gas in the lower part of Figure S1. The adsorption complexes were observed, and the reaction was as follows:

$$PtC_{4-6}^- + N_2 \rightarrow PtC_{4-6}N_2^-$$

The photoelectron images and the corresponding photoelectron spectra of PtC_n^- and $PtC_nN_2^-$ (n = 4−6) recorded at 266 nm are shown in Figure 1. The maximum value of the dominant band marked with X corresponds to the VDEs of the ground state, which is directly measured to be 3.48 ± 0.06 (PtC_4^-), 2.66 ± 0.10 (PtC_5^-), 3.82 ± 0.04 (PtC_6^-), 3.80 ± 0.04 ($PtC_4N_2^-$), 2.94 ± 0.08 ($PtC_5N_2^-$), and 4.11 ± 0.02 eV ($PtC_6N_2^-$) (Table 1), respectively. The spectral bands without vibrationally resolved structures prevent us from directly measuring the ground-state ADEs, which can be alternatively

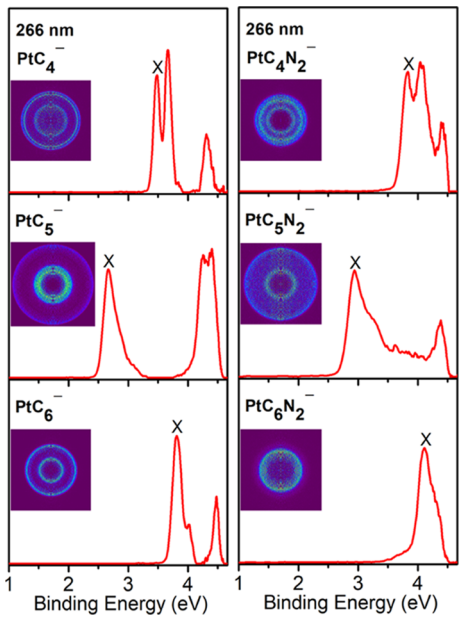

Figure 1. Photoelectron spectra of PtC_n^- and $PtC_nN_2^-$ (n = 4−6) recorded at 266 nm (4.661 eV). Photoelectron images after inverse Abel transformation are embedded in the photoelectron spectra.

estimated by the intersection of a line drawn along the rising edge of the main band with the binding energy axis. In this way, the ADE value of PtC_n^- and $PtC_nN_2^-$ (n = 4−6) is evaluated to be 3.34 ± 0.07 (PtC_4^-), 2.53 ± 0.11 (PtC_5^-), 3.65 ± 0.05 (PtC_6^-), 3.67 ± 0.05 ($PtC_4N_2^-$), 2.80 ± 0.09 ($PtC_5N_2^-$), and 3.93 ± 0.04 eV ($PtC_6N_2^-$) (Table 1), respectively. Interestingly, a larger gap between the ground state peak and the excited state peak was observed in the spectra of PtC_5^- and $PtC_5N_2^-$ as compared with other species, indicating that the PtC_5 and PtC_5N_2 neutrals have a large gap between their highest occupied molecular orbital (HOMO) and lowest unoccupied molecular orbital.[51−54]

3.2. Comparison between Experimental and Theoretical Results. Ground-state structures and selected low-lying isomers for PtC_n^- and $PtC_nN_2^-$ (n = 4−6) anions are shown in Figure 2. Each complex was considered with three isomers with relatively low energies, respectively.

For PtC_4^-, the lowest-lying isomer (labeled 4A) is in $C_{\infty v}$ symmetry and exhibits a linear chain structure with a $^2\Sigma^+$ electronic state. The 4B isomer is 1.41 eV higher in energy than 4A, which has a C_{2v} symmetry with a carbon triangle structure and a $^2A_1$ electronic state. Isomer 4C lies 1.42 eV higher above isomer 4A and has C_s symmetry with an electronic state of $^4A'$ electronic state. The calculated VDE and ADE values of 4A (3.45 and 3.33 eV) agree well with the experimental values (3.48 ± 0.06 and 3.34 ± 0.07 eV) (Table 1). The VDEs and ADEs of 4B (3.39 and 2.72 eV) and 4C (2.07 and 2.02 eV) do not match the experimental values. In addition, the energies of 4B and 4C isomers are too high to be detected in the experiment.

For $PtC_4N_2^-$, in the lowest-lying isomer (labeled 4a), N_2 is bound to the Pt atom in an end-on $C_{\infty v}$ configuration. In isomer 4b with 0.49 eV higher energy, N_2 is completely cleaved, forming a C_s configuration with two stable carbon−nitrogen bonds. Isomer 4c lies 1.46 eV higher as compared to isomer 4a, in which N_2 is completely cleaved, forming a cricoid C_{2v} configuration. The calculated VDE/ADE values of 4a are

https://doi.org/10.1021/acs.inorgchem.2c03150
Inorg. Chem. 2023, 62, 170−177

Table 1. Comparison of Experimental VDE and ADE Values to B3LYP Calculated Ones of the Three Lowest-Energy Isomers for PtC_n^- and $PtC_nN_2^-$ (n = 4–6)

			VDE (eV)		ADE (eV)	
cluster	isomer	relative energy (eV)	expt.[a]	calc.	expt.[a]	calc.
PtC_4^-	4A	0.00	3.48(6)	3.45	3.34(7)	3.33
	4B	1.41		3.39		2.72
	4C	1.42		2.07		2.02
PtC_5^-	5A	0.00	2.66(10)	2.63	2.53(11)	2.60
	5B	0.85		3.35		3.29
	5C	1.20		3.70		3.40
PtC_6^-	6A	0.00	3.82(4)	3.73	3.65(5)	3.60
	6B	1.07		3.34		2.91
	6C	1.23		3.65		3.22
$PtC_4N_2^-$	4a	0.00	3.80(4)	3.90	3.67(5)	3.70
	4b	0.49		3.95		3.82
	4c	1.46		2.84		2.74
$PtC_5N_2^-$	5a	0.00	2.94(8)	3.10	2.80(9)	2.95
	5b	0.82		3.91		3.80
	5c	0.89		3.89		3.75
$PtC_6N_2^-$	6a	0.00	4.11(2)	4.13	3.93(4)	4.03
	6b	1.25		3.42		3.26
	6c	1.40		4.11		4.00

[a]Numbers in parentheses represent the uncertainty in the last digit.

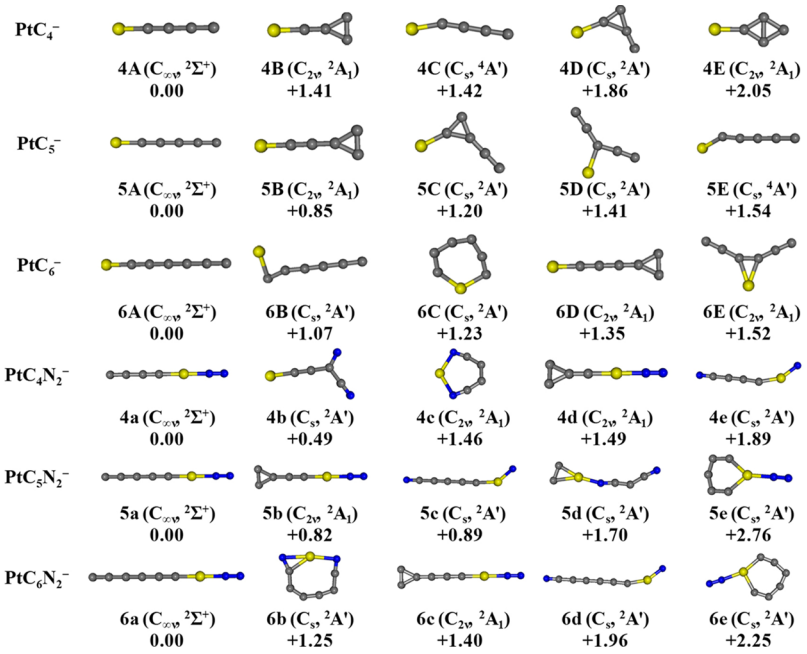

Figure 2. Ground-state structures and selected low-lying isomers for PtC_n^- and $PtC_nN_2^-$ (n = 4–6) anions calculated at the B3LYP/aug-cc-pVTZ/aug-cc-pVTZ-PP level.

3.90/3.70 eV, which are in agreement with the experimental values of 3.80 ± 0.04/3.67 ± 0.05 eV. The calculated VDE/ADE values of isomers 4b (3.95/3.82 eV) deviate slightly from the experimental values, whereas those of 4c (2.84/2.74 eV) differ remarkably from the experimental values.

For PtC_5^-, the lowest-lying isomer, labeled as 5A, has a linear chain structure with a $^2\Sigma^+$ ground state (Figure 2). The calculated VDE and ADE of 5A is 2.63 and 2.60 eV (Table 1), respectively, which is consistent with the corresponding experimental value (2.66 ± 0.10 and 2.53 ± 0.11 eV). The 5B isomer is 0.85 eV higher in energy than 5A, which has a carbon triangle structure with $^2A_1$ electronic state and C_{2v} symmetry. The calculated VDE and ADE of 5B is 3.35 and 3.29 eV, respectively, which is quite different from the experiment. Isomer 5C has C_s symmetry with an electronic state of $^2A'$ electronic state, and it lies 1.20 eV higher above isomer 5A. The calculated VDE and ADE value (3.70 and 3.40 eV) is also obviously higher than the experimental value. Therefore, the 5A isomer should contribute to the experimental spectrum, while the presence of 5B and 5C can be ruled out.

For $PtC_5N_2^-$, in the most stable isomer 5a, N_2 is bound to the Pt atom in an end-on $C_{\infty v}$ configuration with a $^2\Sigma^+$ ground state. The calculated VDE and ADE value of the 5a isomer is

https://doi.org/10.1021/acs.inorgchem.2c03150
Inorg. Chem. 2023, 62, 170–177

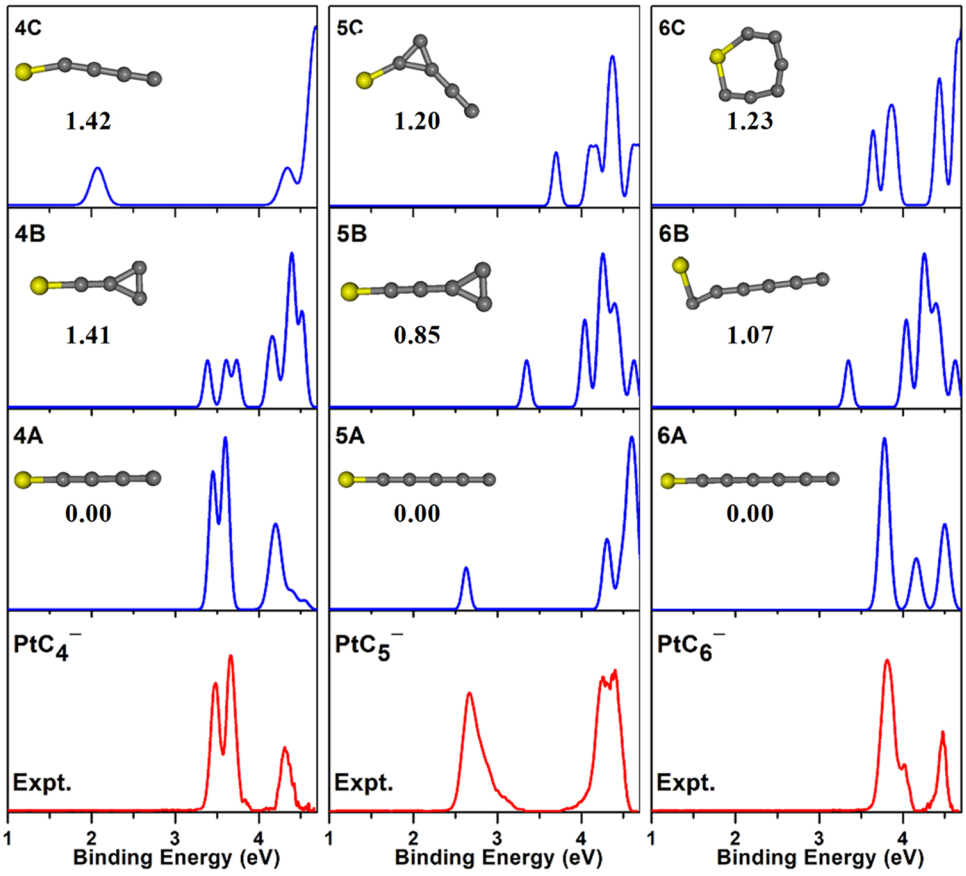

Figure 3. Comparison of experimental 266 nm photoelectron spectra (bottom rows) of PtC_n^- (n = 4−6) to the simulated spectra of the low-lying isomers (top rows). Structures and relative energies are embedded in it.

3.10 and 2.95 eV, respectively, which is in reasonable agreement with the experimental values (2.94 ± 0.08 and 2.80 ± 0.09 eV). The 5b isomer in C_{2v} symmetry contains a carbon triangle structure with a $^2A_1$ ground state, in which N_2 is bound to the Pt atom in an end-on configuration. In the 5c isomer, N_2 is completely cleaved with a chain structure in that two N atoms are on opposite sides. The 5b and 5c isomers lie 0.82 and 0.89 eV higher in energy than 5a, respectively. The VDE/ADE values of 5b (3.91 and 3.80 eV) and 5c (3.89 and 3.75 eV) differ greatly from the experimental values (2.94 and 2.80 eV). It thus appears that 5a is responsible for the experimental spectrum.

For the n = 6 cluster, the lowest-energy isomer of PtC_6^- (6A) displays a linear chain structure with a $^2\Sigma^+$ electronic state. The 6B isomer in C_s symmetry contains a curved chain structure with a $^2A'$ ground state. The 6C isomer is featured by a ring structure with a C_s symmetry. The 6B and 6C isomers lie 1.07 and 1.23 eV higher than 6A, respectively. The calculated VDE and ADE of the most stable isomer 6A are 3.73 and 3.60 eV, which are in good agreement with the experimental values of 3.82 ± 0.04/3.65 ± 0.05 eV. The VDE and ADE of 6B (3.34 and 2.91 eV) and 6C (3.65 and 3.22 eV) differ from the experimental value. The 6B and 6C isomers are too high to be detected experimentally.

For $PtC_6N_2^-$, the most stable isomer (6a) consists of a $C_{\infty v}$ structure with a $^2\Sigma^+$ ground state. In the 6a isomer, N_2 is bound to the Pt atom in an end-on configuration. The calculated VDE/ADE of isomer 6a is 4.13/4.03 eV (Table 1), respectively, which is consistent with the corresponding experimental value (4.11 ± 0.02 and 3.93 ± 0.04 eV). The 6b isomer is 1.25 eV higher in energy than 6a, which has a C_s symmetry and a $^2A'$ electronic state. In the 6b isomer, N_2 is completely cleaved, forming an annular structure with two stable carbon−nitrogen bonds. The 6c isomer lies 1.40 eV higher in energy than isomer 6a, which has a C_{2v} symmetry and contains a carbon triangle structure with a $^2A_1$ ground state, and N_2 is bound to the Pt atom in an end-on configuration. The VDE/ADE of 6b (3.42/3.26 eV) is much lower than the experimental value. The 6b and 6c isomers lie too high in energy to be experimentally probed.

4. DISCUSSION

In order to further verify the structural characteristics, we compared the 266 nm experimental photoelectron spectra of PtC_n^- and $PtC_nN_2^-$ (n = 4−6) with the simulated density of state spectra of the most stable isomers, as shown in Figures 3 and 4. It can be seen that energy band positions and overall spectra of the most stable isomers of PtC_n^- and $PtC_nN_2^-$ (n = 4−6) are in reasonable agreement with the experimental spectral characteristics, indicating that these lowest-energy structures should be responsible for the observed spectral features under the current experimental conditions. Furthermore, these anion clusters are typically characterized by linear chain geometry. The consistency between the theoretical and experimental results allows for establishment of the structural features of PtC_n^- and $PtC_nN_2^-$ (n = 4−6).

The bond lengths of N−N bonds in these clusters are listed in Table 2. Throughout the reaction, the bond lengths of the

https://doi.org/10.1021/acs.inorgchem.2c03150
Inorg. Chem. 2023, 62, 170−177

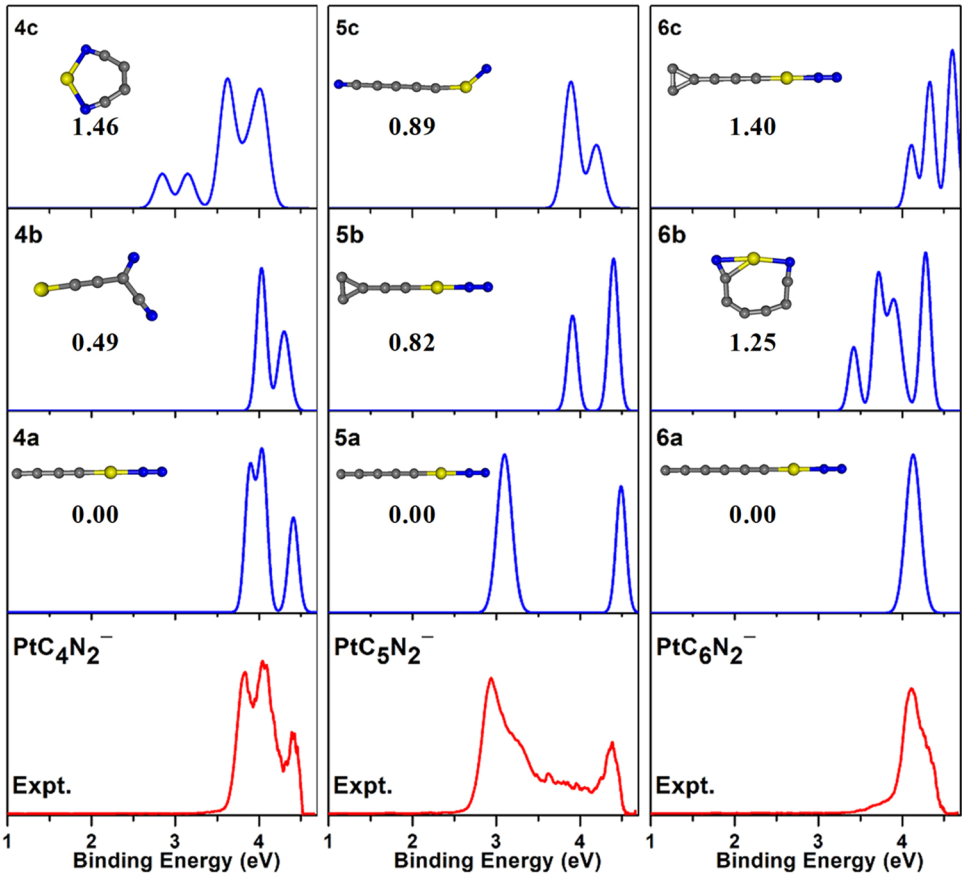

Figure 4. Comparison of experimental 266 nm photoelectron spectra (bottom rows) of $PtC_nN_2^-$ (n = 4−6) to the simulated spectra of the low-lying isomers (top rows). Structures and relative energies are embedded in it.

Table 2. N−N Wiberg Bond Orders, N−N Bond Lengths, and Natural Population Analysis (NPA) Charges of the PtC_n^- and $PtC_nN_2^-$ (N = 4−6) Species Calculated at the B3LYP Level

	bond order	bond length	NPA charge		
species	N−N	N−N	Pt	C_n (n = 4−6)	N_2
PtC_4^- + N_2	3.000	1.095	−0.234	−0.766	0.000
$PtC_4N_2^-$	2.680	1.111	−0.160	−0.734	−0.106
PtC_5^- + N_2	3.000	1.095	−0.244	−0.756	0.000
$PtC_5N_2^-$	2.678	1.112	−0.177	−0.715	−0.108
PtC_6^- + N_2	3.000	1.095	−0.208	−0.792	0.000
$PtC_6N_2^-$	2.697	1.110	−0.157	−0.757	−0.086

N−N bond go from 1.095 Å (nitrogen molecule) to 1.111 ($PtC_4N_2^-$), 1.112 ($PtC_5N_2^-$), and 1.110 Å ($PtC_6N_2^-$), indicating that the N−N bond is weakened. The Wiberg bond orders of the N−N bond are 2.680, 2.678, and 2.697 in $PtC_nN_2^-$ (n = 4−6), respectively (Table 2), which are smaller than that of the dissociative nitrogen molecule (3.000). This indicates that PtC_n^- (n = 4−6) contributes to the dinitrogen activation. In order to visualize the charge changes among these atoms (Table 2), NPA was carried out. In the system of n = 4, the amount of negative charge of Pt and C_4 groups decreases with the N_2 addition to the cluster (Pt, from −0.234 to −0.160; C_4, from −0.766 to −0.734), while the amount of negative charge of the N_2 group increases (N_2, from 0 to −0.106). That is, the charge transfer occurs between Pt and C_4 and N_2 groups. Both n = 5 (Pt, from −0.244 to −0.177; C_n, from −0.756 to −0.715; N_2, from 0 to −0.108) and n = 6 (Pt, from −0.208 to −0.157; C_n, from −0.792 to −0.757; N_2, from 0 to −0.086) systems are identical with the abovementioned phenomenon. It turns out that there is a charge transfer between PtC_n^- and N_2 to form $PtC_nN_2^-$ where the Pt and C_n groups transfer electrons to the N_2 group (n = 4−6). These results indicate that N_2 is activated in the reactions between PtC_n^- and N_2.

To study the mechanism of nitrogen fixation and activation, CMO analysis was performed for the $PtC_nN_2^-$ (n = 4−6) anion complexes. Molecular orbital pictures of the most stable isomers are illustrated in Figure 5. On the whole, $PtC_4N_2^-$ and $PtC_6N_2^-$ have similar properties. In the orbitals of HOMO, HOMO−1, HOMO−6, and HOMO−7, the N−N bond shows the π antibonding orbits (π^*). As for HOMO, HOMO−1 can be viewed as π back-donation from the lone electron of 5d orbital in Pt atom into the π antibonding orbits of N_2 (referred to as nπ^*). In HOMO−6 and HOMO-7, Pt atom and C atom form the π bond, which leads to the weakening of nπ^*, and this process can also be understood as contribution from the π electron of the π bond into the antibonding π orbits of N_2 in $PtC_4N_2^-$ and $PtC_6N_2^-$ (referred to as $\pi\pi^*$). More interestingly, the photoelectron spectroscopy of $PtC_5N_2^-$ is particularly compared with that of $PtC_4N_2^-$ and $PtC_6N_2^-$. Also, its molecular orbital is also obviously different from $PtC_4N_2^-$ and $PtC_6N_2^-$. For $PtC_5N_2^-$, HOMO, HOMO−4, and HOMO−5 can be regarded as π back-donation from the lone electron of 5d orbital in Pt atom into the antibonding π orbits of N_2 (referred to as nπ^*). On this basis, the

https://doi.org/10.1021/acs.inorgchem.2c03150
Inorg. Chem. 2023, 62, 170−177

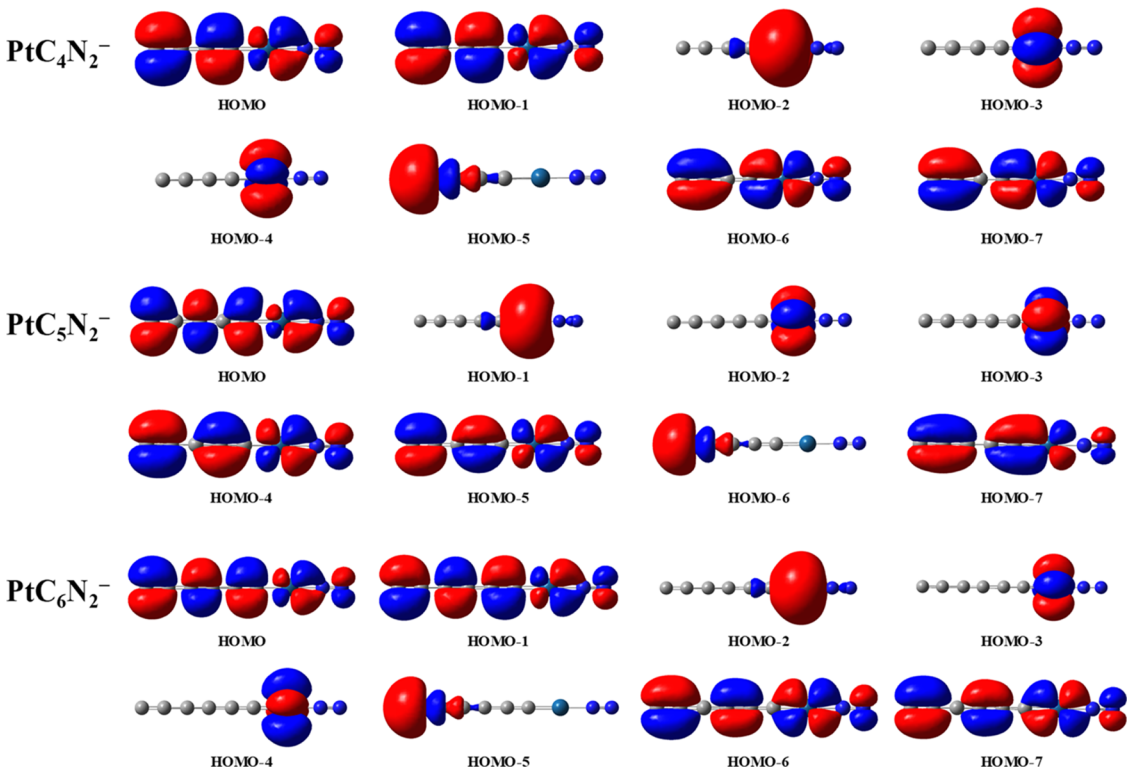

Figure 5. Molecular orbital pictures of the most stable isomers for $PtC_nN_2^-$ (n = 4−6), showing the highest occupied molecular orbitals (HOMO) down to the seventh valence molecular orbital from the HOMO.

combination of bond orders, bond lengths, and NPA charges shows that nπ^* is slightly more effective than $\pi\pi^*$ in weakening the N≡N bond in this system. Previous investigations have proved that π back-donation weakens the N≡N bond, which is crucial for its subsequent fixation and activation. In conclusion, it is evidenced once again that the π back-donation of the 5d orbital of Pt to the antibonding π orbits of N_2 is conducive to the fixation and activation of nitrogen.

5. CONCLUSIONS

Mass spectrometry, photoelectron spectroscopy, and quantum chemical calculations have been carried out to elucidate the electronic and geometric structures of PtC_n^- and $PtC_nN_2^-$ (n = 4−6). The most stable structures of PtC_n^- and $PtC_nN_2^-$ (n = 4−6) are determined to have linear chain structures. For $PtC_nN_2^-$, chemical bonding analyses show that the fixation and activation of dinitrogen is facilitated by the charge transfer from Pt and C_n to N_2. Simultaneously, the significance of the π back-donation of the 5d orbital of Pt to the antibonding π orbits of N_2 for dinitrogen fixation and activation is emphasized. We find that nπ^* is slightly more effective than $\pi\pi^*$ in weakening the N≡N bond in this system. This study identified $PtC_nN_2^-$ species as an indispensable intermediate in the nitrogen fixation process of the mononuclear metal carbide PtC_n^- (n = 4−6) anion cluster, which provides a potential direction for inorganic nitrogen fixation.

■ ASSOCIATED CONTENT

Supporting Information

The Supporting Information is available free of charge at https://pubs.acs.org/doi/10.1021/acs.inorgchem.2c03150.

Mass spectra of the PtC_n^- and $PtC_nN_2^-$ (n = 4−6) complexes (PDF)

■ AUTHOR INFORMATION

Corresponding Author

Hua Xie − *State Key Laboratory of Molecular Reaction Dynamics, Dalian Institute of Chemical Physics, Chinese Academy of Sciences, Dalian 116023, China;* orcid.org/0000-0003-2091-6457; Email: xiehua@dicp.ac.cn

Authors

Shihu Du − *State Key Laboratory of Molecular Reaction Dynamics, Dalian Institute of Chemical Physics, Chinese Academy of Sciences, Dalian 116023, China; School of Mathematics and Physics, Hebei University of Engineering, Handan 056038, China*

Xuegang Liu − *State Key Laboratory of Molecular Reaction Dynamics, Dalian Institute of Chemical Physics, Chinese Academy of Sciences, Dalian 116023, China*

Bangmin Ju − *State Key Laboratory of Molecular Reaction Dynamics, Dalian Institute of Chemical Physics, Chinese Academy of Sciences, Dalian 116023, China*

Jumei Zhang − *School of Life Science, Ludong University, Yantai, Shandong 264025, China*

Jinghan Zou − *State Key Laboratory of Molecular Reaction Dynamics, Dalian Institute of Chemical Physics, Chinese Academy of Sciences, Dalian 116023, China*

Gang Li − *State Key Laboratory of Molecular Reaction Dynamics, Dalian Institute of Chemical Physics, Chinese Academy of Sciences, Dalian 116023, China;* orcid.org/0000-0001-5984-111X

Hongjun Fan − *State Key Laboratory of Molecular Reaction Dynamics, Dalian Institute of Chemical Physics, Chinese Academy of Sciences, Dalian 116023, China;* orcid.org/0000-0003-3406-6932

https://doi.org/10.1021/acs.inorgchem.2c03150
Inorg. Chem. 2023, 62, 170−177

Ling Jiang − *State Key Laboratory of Molecular Reaction Dynamics, Dalian Institute of Chemical Physics, Chinese Academy of Sciences, Dalian 116023, China;* orcid.org/0000-0002-8485-8893

Complete contact information is available at: https://pubs.acs.org/10.1021/acs.inorgchem.2c03150

Author Contributions

S.D. and X.L. contributed equally to this work and share the first authorship.

Notes

The authors declare no competing financial interest.

■ ACKNOWLEDGMENTS

The authors gratefully acknowledge the Dalian Coherent Light Source (DCLS) for support and assistance. This work was supported by the National Natural Science Foundation of China (Grant Nos. 21873097, 22125303, 92061203, and 22288201), the Youth Innovation Promotion Association of the Chinese Academy of Sciences (CAS) (2020187), the Dalian Young Star of Science and Technology Project (No. 2021RQ128), the Strategic Priority Research Program of CAS (XDB17000000), CAS (GJJSTD20190002), and K. C. Wong Education Foundation (GJTD-2018-06).

■ REFERENCES

(1) Erisman, J. W.; Sutton, M. A.; Galloway, J.; Klimont, Z.; Winiwarter, W. How a century of ammonia synthesis changed the world. *Nat. Geosci.* **2008**, *1*, 636−639.
(2) Tanaka, H.; Nishibayashi, Y.; Yoshizawa, K. Interplay between Theory and Experiment for Ammonia Synthesis Catalyzed by Transition Metal Complexes. *Acc. Chem. Res.* **2016**, *49*, 987−995.
(3) Schrock, D. V. Y. Catalytic Reduction of Dinitrogen to Ammonia at a Single Molybdenum Center. *Science* **2003**, *301*, 76−78.
(4) Weare, W. W.; Dai, X.; Byrnes, M. J.; Chin, J. M.; Schrock, R. R.; Muller, P. Catalytic reduction of dinitrogen to ammonia at a single molybdenum center. *Proc. Natl. Acad. Sci. U. S. A.* **2006**, *103*, 17099−17106.
(5) Arashiba, K.; Miyake, Y.; Nishibayashi, Y. A molybdenum complex bearing PNP-type pincer ligands leads to the catalytic reduction of dinitrogen into ammonia. *Nat. Chem.* **2011**, *3*, 120−125.
(6) John, S.; Anderson, J. R. Catalytic conversion of nitrogen to ammonia by an iron model complex. *Nature* **2013**, *501*, 84−87.
(7) Kafizas, A.; Carmalt, C. J.; Ivan, P. P. CVD and precursor chemistry of transition metal nitrides. *Coord. Chem. Rev.* **2013**, *257*, 2073−2119.
(8) Zerr, A.; Miehe, G.; Riedel, R. Synthesis of cubic zirconium and hafnium nitride having Th_3P_4 structure. *Nat. Mater.* **2003**, *2*, 185−189.
(9) Braun, T. Oxidative addition of NH_3 to a transition-metal complex: a key step for the metal-mediated derivatization of ammonia? *Angew. Chem., Int. Ed.* **2005**, *44*, 5012−5014.
(10) Diederich, F. 25 years full of chemical discovery. *Angew. Chem., Int. Ed.* **2011**, *50*, 8−12.
(11) Zhou, S.; Li, J.; Schlangen, M.; Schwarz, H. Efficient Room-Temperature Activation of Methane by TaN^+ under C-N Coupling. *Angew. Chem., Int. Ed.* **2016**, *55*, 11678−11681.
(12) Zhou, S.; Li, J.; Schlangen, M.; Schwarz, H. Thermische Dehydrierung von Methan durch $[ReN]^+$. *Angew. Chem., Int. Ed.* **2016**, *128*, 15085−15089.
(13) Zhou, S.; Sun, X.; Yue, L.; Guo, C.; Schlangen, M.; Schwarz, H. Selective Nitrogen-Atom Transfer Driven by a Highly Efficient Intersystem Crossing in the $[CeON]^+$ /CH_4 System. *Angew. Chem., Int. Ed.* **2018**, *57*, 15902−15906.
(14) Xiaoyan, S.; Zhou, S.; Yue, L.; Guo, C.; Schlangen, M.; Schwarz, H. On the Remarkable Role of the Nitrogen Ligand in the Gas-Phase Redox Reaction of the N_2O/CO Couple Catalyzed by $[NbN]^+$. *Angew. Chem., Int. Ed.* **2019**, *58*, 3635−3639.
(15) Lv, Z.-J.; Wei, J.; Zhang, W.-X.; Chen, P.; Deng, D.; Shi, Z.-J.; Xi, Z. Direct transformation of dinitrogen: synthesis of N-containing organic compounds via N−C bond formation. *Nat. Sci. Rev.* **2020**, *7*, 1564−1583.
(16) Dillinger, S.; Klein, M. P.; Steiner, A.; McDonald, D. C.; Duncan, M. A.; Kappes, M. M.; Niedner-Schatteburg, G. Cryo IR Spectroscopy of N_2 and H_2 on Ru_8^+ The Effect of N_2 on the H-Migration. *J. Phys. Chem. Lett.* **2018**, *9*, 914−918.
(17) Liu, G.; Ariyarathna, I. R.; Ciborowski, S. M.; Zhu, Z.; Miliordos, E.; Bowen, K. H. Simultaneous Functionalization of Methane and Carbon Dioxide Mediated by Single Platinum Atomic Anions. *J. Am. Chem. Soc.* **2020**, *142*, 21556−21561.
(18) Liu, G.; Poths, P.; Zhang, X.; Zhu, Z.; Marshall, M.; Blankenhorn, M.; Alexandrova, A. N.; Bowen, K. H. CO_2 Hydrogenation to Formate and Formic Acid by Bimetallic Palladium-Copper Hydride Clusters. *J. Am. Chem. Soc.* **2020**, *142*, 7930−7936.
(19) Levin, N.; Lengyel, J.; Eckhard, J. F.; Tschurl, M.; Heiz, U. Catalytic Non-Oxidative Coupling of Methane on TaO. *J. Am. Chem. Soc.* **2020**, *142*, 5862−5869.
(20) Asher, R. L.; Bellert, D.; Buthelezi, T.; Brucat, P. J. Optical Excitation of Co^+N_2. *J. Phys. Chem.* **1995**, *99*, 1068−1072.
(21) Berces, A.; Hackett, P. A.; Lian, L.; Mitchell, S. A.; Rayner, D. M. Reactivity of niobium clusters with nitrogen and deuterium. *J. Chem. Phys.* **1998**, *108*, 5476−5490.
(22) Salahub, H. A. D. $Fe(N_2)_n$ (n = 1-5): Structure, Bonding, and Vibrations from Density Functional Theory. *Inorg. Chem.* **1999**, *38*, 3895−3903.
(23) Kim, Y. D. Non-dissociative adsorption of diatomic molecules on nanoclusters at room temperature. *Chem. Phys. Lett.* **2003**, *382*, 644−649.
(24) Kim, Y. D. Formation of activated diatomic species on mass-selected clusters. *J. Mol. Struct.* **2004**, *692*, 139−144.
(25) Pillai, E. D.; Jaeger, T. D.; Duncan, M. A. IR Spectroscopy and Density Functional Theory of Small $V^+(N_2)_n$ Complexes. *J. Phys. Chem. A* **2005**, *109*, 3521−3526.
(26) Dinesh Pillai, E.; Jaeger, T. D.; Duncan, M. A. IR Spectroscopy of $Nb^+(N_2)_n$ Complexes: Coordination, Structures, and Spin States. *J. Am. Chem. Soc.* **2007**, *129*, 2297−2307.
(27) Heim, H. C.; Bernhardt, T. M.; Lang, S. M.; Barnett, R. N.; Landman, U. Interaction of Iron−Sulfur Clusters with N_2: Biomimetic Systems in the Gas Phase. *J. Phys. Chem. C* **2016**, *120*, 12549−12558.
(28) Xie, H.; Shi, L.; Xing, X.; Tang, Z. Infrared photodissociation spectroscopy of $M(N_2)_n^+$ (M = Y, La, Ce; n = 7-8) in the gas phase. *Phys. Chem. Chem. Phys.* **2016**, *18*, 4444−4450.
(29) Deng, G.; Pan, S.; Wang, G.; Zhao, L.; Zhou, M.; Frenking, G. Side-On Bonded Beryllium Dinitrogen Complexes. *Angew. Chem., Int. Ed.* **2020**, *59*, 10603−10609.
(30) Geng, L.; Jia, Y.; Zhang, H.; Cui, C.; Luo, Z. Plasma-Assisted Dinitrogen Activation on Small Cobalt Clusters: $Co_4N_9^+$ with Enhanced Stability. *ChemPhysChem* **2022**, *23*, No. e202200288.
(31) Li, Z.-Y.; Mou, L.-H.; Wei, G.-P.; Ren, Y.; Zhang, M.-Q.; Liu, Q.-Y.; He, S.-G. C-N Coupling in N_2 Fixation by the Ditantalum Carbide Cluster Anions $Ta_2C_4^-$. *Inorg. Chem.* **2019**, *58*, 4701−4705.
(32) Mou, L.-H.; Li, Y.; Li, Z.-Y.; Liu, Q.-Y.; Ren, Y.; Chen, H.; He, S.-G. Dinitrogen Activation and Functionalization by Heteronuclear Metal Cluster Anions $FeV_2C_2^-$ at Room Temperature. *J. Phys. Chem. Lett.* **2020**, *11*, 9990−9994.
(33) Leigh, G. J. Protonation of Coordinated Dinitrogen. *Acc. Chem. Res.* **1992**, *25*, 178−181.
(34) Holland, P. L. Metal-dioxygen and metal-dinitrogen complexes: where are the electrons? *Dalton Trans.* **2010**, *39*, 5415−5425.
(35) Fryzuk, R. J. B. Examining the relationship between coordination mode and reactivity of dinitrogen. *Nat. Rev. Chem.* **2017**, *1*, No. 0026.
(36) Cheng, X.; Li, Z.-Y.; Mou, L.-H.; Ren, Y.; Liu, Q.-Y.; Ding, X.-L.; He, S.-G. Side-on-End-on Coordination of Dinitrogen on a

Polynuclear Vanadium Nitride Cluster Anion $[V_5N_5]^-$. *Chem. – Eur. J.* **2019**, *25*, 16523–16527.
(37) Li, Z.-Y.; Li, Y.; Mou, L.-H.; Chen, J.-J.; Liu, Q.-Y.; He, S.-G.; Chen, H. A Facile N-N Bond Cleavage by the Trinuclear Metal Center in Vanadium Carbide Cluster Anions $V_3C_4^-$. *J. Am. Chem. Soc.* **2020**, *142*, 10747–10754.
(38) Jiang, G.-D.; Li, Z.-Y.; Mou, L.-H.; He, S.-G. Dual Iron Sites in Activation of N_2 by Iron-Sulfur Cluster Anions $Fe_5S_2^-$ and $Fe_5S_3^-$. *J. Phys. Chem. Lett.* **2021**, *12*, 9269–9274.
(39) Wang, M.; Chu, L.-Y.; Li, Z.-Y.; Messinis, A. M.; Ding, Y.-Q.; Lianrui, H.; Ma, J.-B. Dinitrogen and Carbon Dioxide Activation to Form C-N Bonds at Room Temperature: A New Mechanism Revealed by Experimental and Theoretical Studies. *J. Phys. Chem. Lett.* **2021**, *12*, 3490–3496.
(40) Geng, C.; Li, J.; Weiske, T.; Schwarz, H. Ta_2^+-mediated ammonia synthesis from N_2 and H_2 at ambient temperature. *Proc. Natl. Acad. Sci. U. S. A.* **2018**, *115*, 11680–11687.
(41) Geng, C.; Li, J.; Weiske, T.; Schwarz, H. Complete cleavage of the N≡N triple bond by Ta_2N^+ via degenerate ligand exchange at ambient temperature: A perfect catalytic cycle. *Proc. Natl. Acad. Sci. U. S. A.* **2019**, *116*, 21416–21420.
(42) Zhao, Y.; Cui, J.-T.; Wang, M.; Valdivielso, D. Y.; Fielicke, A.; Hu, L.-R.; Cheng, X.; Liu, Q.-Y.; Li, Z.-Y.; He, S.-G.; Ma, J.-B. Dinitrogen Fixation and Reduction by $Ta_3N_3H_{0,1}^-$ Cluster Anions at Room Temperature: Hydrogen-Assisted Enhancement of Reactivity. *J. Am. Chem. Soc.* **2019**, *141*, 12592–12600.
(43) Mou, L.-H.; Li, Y.; Li, Z.-Y.; Liu, Q.-Y.; Chen, H.; He, S.-G. Dinitrogen Activation by Heteronuclear Metal Carbide Cluster Anions $FeTaC_2^-$: A 5d Early and 3d Late Transition Metal Strategy. *J. Am. Chem. Soc.* **2021**, *143*, 19224–19231.
(44) Cheng, X.; Li, Z.-Y.; Mou, L.-H.; Wei, G.-P.; Liu, Q.-Y.; He, S.-G. Size-dependent reactivity of rhodium deuteride cluster anions $Rh_3D_n^-$ (n = 0-3) toward dinitrogen: The prominent role of sigma donation. *J. Chem. Phys.* **2022**, *156*, No. 064303.
(45) Qin, Z.; Wu, X.; Tang, Z. Note: a novel dual-channel time-of-flight mass spectrometer for photoelectron imaging spectroscopy. *Rev. Sci. Instrum.* **2013**, *84*, No. 066108.
(46) Frisch, M. J.; Trucks, G. W.; Schlegel, H. B.; Scuseria, G. E.; Robb, M. A.; Cheeseman, J. R.; Scalmani, G.; Barone, V.; Mennucci, B.; Petersson, G. A.; Nakatsuji, H.; Caricato, M.; Li, X.; Hratchian, H. P.; Izmaylov, A. F.; Bloino, J.; Zheng, G.; Sonnenberg, J. L.; Hada, M.; Ehara, M.; Toyota, K.; Fukuda, R.; Hasegawa, J.; Ishida, M.; Nakajima, T.; Honda, Y.; Kitao, O.; Nakai, H.; Vreven, T.; Montgomery, Jr., J. A.; Peralta, J. E.; Ogliaro, F.; Bearpark, M. J.; Heyd, J.; Brothers, E. N.; Kudin, K. N.; Staroverov, V. N.; Kobayashi, R.; Normand, J.; Raghavachari, K.; Rendell, A. P.; Burant, J. C.; Iyengar, S. S.; Tomasi, J.; Cossi, M.; Rega, N.; Millam, N. J.; Klene, M.; Knox, J. E.; Cross, J. B.; Bakken, V.; Adamo, C.; Jaramillo, J.; Gomperts, R.; Stratmann, R. E.; Yazyev, O.; Austin, A. J.; Cammi, R.; Pomelli, C.; Ochterski, J. W.; Martin, R. L.; Morokuma, K.; Zakrzewski, V. G.; Voth, G. A.; Salvador, P.; Dannenberg, J. J.; Dapprich, S.; Daniels, A. D.; Farkas, O.; Foresman, J. B.; Ortiz, J. V.; Cioslowski, J.; Fox, D. J.*Gaussian 09*; Gaussian, Inc.: Wallingford, CT, 2009.
(47) Dunning, T. H. Gaussian basis sets for use in correlated molecular calculations. I. The atoms boron through neon and hydrogen. *J. Chem. Phys.* **1989**, *90*, 1007–1023.
(48) Becke, A. D. Density-functional thermochemistry. III. The role of exact exchange. *J. Chem. Phys.* **1993**, *98*, 5648.
(49) Lee, C.; Yang, W.; Parr, R. G. Development of the Colle-Salvetti correlation-energy formula into a functional of the electron density. *Phys. Rev. B: Condens. Matter Mater. Phys.* **1988**, *37*, 785–789.
(50) Glendening, E. D.; Reed, A. E.; Carpenter, J. E.; Weinhold, F.*NBO 3.1*; Theoretical Chemistry Institute, 1998.
(51) Wang, P.; Zhang, W.; Xu, X.-L.; Yuan, J.; Xu, H.-G.; Zheng, W. Gas phase anion photoelectron spectroscopy and theoretical investigation of gold acetylide species. *J. Chem. Phys.* **2017**, *146*, 194303.
(52) Yang, S. H.; Pettiette, C. L.; Conceicao, J.; Cheshnovsky, O.; Smalley, R. E. UPS of Buckminsterfullerene and other large clusters of carbon. *Chem. Phys. Lett.* **1987**, *139*, 233–238.
(53) Li, X.; Grubisic, A.; Stokes, S. T.; Cordes, J.; Ganteför, G. F.; Bowen, K. H.; Kiran, B.; Willis, M.; Jena, P.; Burgert, R.; Schnöckel, H. Unexpected Stability of Al_4H_6: A Borane Analog? *Science* **2007**, *315*, 356–358.
(54) Lu, S.-J.; Xu, X. L.; Xu, H.-G.; Zheng, W.-J. Structures and bonding properties of $CPt_2^{-/0}$ and $CPt_2H^{-/0}$: Anion photoelectron spectroscopy and quantum chemical calculations. *J. Chem. Phys.* **2019**, *151*, 224303.

https://doi.org/10.1021/acs.inorgchem.2c03150
Inorg. Chem. 2023, 62, 170–177